

Journal of Geophysical Research: Biogeosciences

RESEARCH ARTICLE

10.1002/2013JG002532

Key Points:

- Global burned area data set was reconstructed by using fire model simulation
- Global burned area showed a downward trend in the twentieth century
- Human and environmental factors were critical in shaping fire regimes

Correspondence to:

H. Tian,
tianhan@auburn.edu

Citation:

Yang, J., H. Tian, B. Tao, W. Ren, J. Kush, Y. Liu, and Y. Wang (2014), Spatial and temporal patterns of global burned area in response to anthropogenic and environmental factors: Reconstructing global fire history for the 20th and early 21st centuries, *J. Geophys. Res. Biogeosci.*, 119, 249–263, doi:10.1002/2013JG002532.

Received 10 OCT 2013

Accepted 9 FEB 2014

Accepted article online 14 FEB 2014

Published online 14 MAR 2014

Spatial and temporal patterns of global burned area in response to anthropogenic and environmental factors: Reconstructing global fire history for the 20th and early 21st centuries

Jia Yang¹, Hanqin Tian¹, Bo Tao¹, Wei Ren¹, John Kush¹, Yongqiang Liu², and Yuhang Wang³

¹International Center for Climate and Global Change Research, School of Forestry and Wildlife Sciences, Auburn University, Auburn, Alabama, USA, ²Center for Forest Disturbance Science, USDA Forest Service, Athens, Georgia, USA, ³School of Earth and Atmospheric Science, Georgia Institute of Technology, Atlanta, Georgia, USA

Abstract Fire is a critical component of the Earth system, and substantially influences land surface, climate change, and ecosystem dynamics. To accurately predict the fire regimes in the 21st century, it is essential to understand the historical fire patterns and recognize the interaction among fire, human, and environment factors. Until now, few efforts are put on the studies regarding to the long-term fire reconstruction and the attribution analysis of anthropogenic and environmental factors to fire regimes at global scale. To fill this knowledge gap, we developed a $0.5^\circ \times 0.5^\circ$ data set of global burned area from 1901 to 2007 by coupling Global Fire Emission Database version 3 with a process-based fire model and conducted factorial simulation experiments to evaluate the impacts of human, climate, and atmospheric components. The average global burned area is $\sim 442 \times 10^4 \text{ km}^2 \text{ yr}^{-1}$ during 1901–2007 and our results suggest a notable declining rate of burned area globally ($1.28 \times 10^4 \text{ km}^2 \text{ yr}^{-1}$). Burned area in tropics and extratropics exhibited a significant declining trend, with no significant trend detected at high latitudes. Factorial experiments indicated that human activities were the dominant factor in determining the declining trend of burned area in tropics and extratropics, and climate variation was the primary factor controlling the decadal variation of burned area at high latitudes. Elevated CO₂ and nitrogen deposition enhanced burned area in tropics and southern extratropics but suppressed fire occurrence at high latitudes. Rising temperature and frequent droughts are becoming increasingly important and expected to increase wildfire activity in many regions of the world.

1. Introduction

Fire plays a critical role in shaping biosphere and atmospheric patterns. Fire regimes are largely regulated by climate [Morton *et al.*, 2013] and human activities [Marlon *et al.*, 2008]; meanwhile, burning of biomass can speed up climate change through altering atmospheric radiative characteristics and land surface albedo [Andreae, 1991; Langmann *et al.*, 2009; Levine *et al.*, 1995; Randerson *et al.*, 2006; Y. Liu *et al.*, 2013]. In the future, the global fire regimes may be quite different from the present pattern due to rapid climate change [Bowman *et al.*, 2009], and anthropogenic effects on fire might become less important than climatic influences [Pechony and Shindell, 2010]. A better understanding of the interaction among fire, climate, and human activities is helpful to enhance our capability of predicting future fire pattern and provide scientific information for fire management policy in the 21st century.

To date, a variety of methods have been used to retrieve fire history at local and regional scales, including charcoal records of biomass burning [Marlon *et al.*, 2008], tree fire scars [Baisan and Swetnam, 1990; Baker and Ehle, 2001; Kitzberger *et al.*, 2007; Niklasson and Granström, 2000; Payette *et al.*, 1989; Wallenius *et al.*, 2004; Westerling and Swetnam, 2003], official fire records [Stocks *et al.*, 2002], and satellite observations [Eidenshink *et al.*, 2007]. At the global scale, gridded burned area has also been estimated through methods grouped into three categories: satellite observation, fire modeling, and hybrid approach. Since the early 1980s, satellite imagery has been widely used to retrieve global fire pattern [Bowman *et al.*, 2009]. Numerous satellite-based global fire products have become available in the recent decade, including Global Burnt Area 2000 (GBA2000) [Grégoire *et al.*, 2003], L3JRC [Tansey *et al.*, 2008], Global Fire Emission Database version 3 (GFED3) [Giglio *et al.*, 2010], and so on. GFED has the longest global fire observation, spanning 15 years from 1997 to 2012, and was

verified by ground fire records in various regions [Giglio *et al.*, 2013; Giglio *et al.*, 2010]. However, studies of global fire patterns prior to the 1980s are lacking.

Recently, process-based fire modeling has provided an effective tool to estimate large-scale fire patterns. It simulates fire activities (e.g., ignition, spread, and extinguishment) while considering critical environmental factors such as climate, land cover, and land management practices [Pechony and Shindell, 2009]. Process-based fire models have been applied in reconstructing global fire history and investigating fire impacts on ecosystems. These models include MC-FIRE [Lenihan *et al.*, 1998], Glob-FIRM [Thonicke *et al.*, 2001], Reg-FIRM [Venevsky *et al.*, 2002], SPITFIRE [Thonicke *et al.*, 2010], Community Land Model (CLM)-Fire [Li *et al.*, 2012], and Canadian Terrestrial Ecosystem Model (CTEM)-Fire [Arora and Boer, 2005]. Model simulated fire patterns are not often consistent with each other. For example, Kloster *et al.* [2010] estimated global fire patterns based on the modified CTEM-Fire model and found a declining trend in burned areas from the 1900s to the 1960s and an increasing trend from the 1970s to the 1990s. However, the estimation by Li *et al.* [2013] based on CLM-Fire model presented a declining trend from the 1870s to the 1990s.

Mouillot and Field [2005] developed a global burned area data set for the twentieth century through a hybrid approach by incorporating satellite information, official fire records, and some fire trend assumptions. Their estimated global burned area was much larger than satellite observations. For example, their estimated global burned area was $722 \times 10^4 \text{ km}^2$ in 1999, while the GFED3 observed $339 \times 10^4 \text{ km}^2$. Current studies regarding century-scale spatial-explicit global fire history have shortcomings that hinder their application to studying fire-climate-human interactions. First, there is considerable disagreement in estimated global burned area with satellite observations in terms of temporal variation and spatial distribution; second, the effects of anthropogenic and environmental factors on fire patterns are difficult to interpret; third, temporal resolutions are relatively low, which is insufficient to study the seasonality of fire activity and emissions. Therefore, an urgent need is to develop a long-term, high-resolution, gridded global burned area database consistent with satellite observations, with a consideration of both long-term climate change and human impacts.

Global fire regimes have experienced extensive anthropogenic and environmental stresses in the twentieth century due to the rapid climate and land use changes [Prentice, 2010]. Anthropogenic impacts have been recognized as the primary factor in controlling the global burned area [Flannigan *et al.*, 2009; Marlon *et al.*, 2008; Pechony and Shindell, 2010]. The impacts of climate variation have also been studied at local, regional, and global levels [e.g., Westerling *et al.*, 2006]. A key message is "Climate variability and fire weather influence wildfire behavior and account for the variability in fire severity at various time scales" [Liu *et al.*, 2010; Liu *et al.*, 2012]. Most previous studies focused on either climate or anthropogenic factors; only a few quantitatively evaluated the impacts of both climate and human activities. Other environmental factors, such as CO₂ and nitrogen deposition, also play important roles in influencing fire regimes, however, are often neglected. To understand the mechanism of fire regimes at global scale, it is essential to quantify the relative contribution of human and multiple environmental factors simultaneously.

The Dynamic Land Ecosystem Model (DLEM) [Tian *et al.*, 2010] is a highly integrated ecosystem model that incorporates biogeochemical cycle and water cycle to estimate the interactions and feedbacks among multiple ecosystem components. In this study, we improved the DLEM by coupling a process-based fire model to estimate global burned area and the feedback of fire to the ecosystem. The objectives of this study are (1) to develop a global historical fire data set at 0.5° resolution at monthly intervals from 1901 to 2007 through integrating the GFED3 burned area information, (2) to present the global and regional fire patterns, and (3) to discuss the determinative factors controlling fire trend and quantify the relative contributions of anthropogenic and multiple environmental factors to global and regional burned areas.

2. Materials and Methods

2.1. The Fire Module of Dynamic Land Ecosystem Model (DLEM-Fire)

The DLEM has been well validated and applied to studying the fluxes and storage of water, carbon, nitrogen, and multiple greenhouse gases at regional and global levels [e.g., Chen *et al.*, 2012; M. Liu *et al.*, 2013; Lu and Tian, 2013; Ren *et al.*, 2012; Tao *et al.*, 2013; Tian *et al.*, 2010; Tian *et al.*, 2011; Tian *et al.*, 2012; Xu *et al.*, 2010; Zhang *et al.*, 2010]. The DLEM-Fire is a process-based fire module built in DLEM. It is capable of estimating

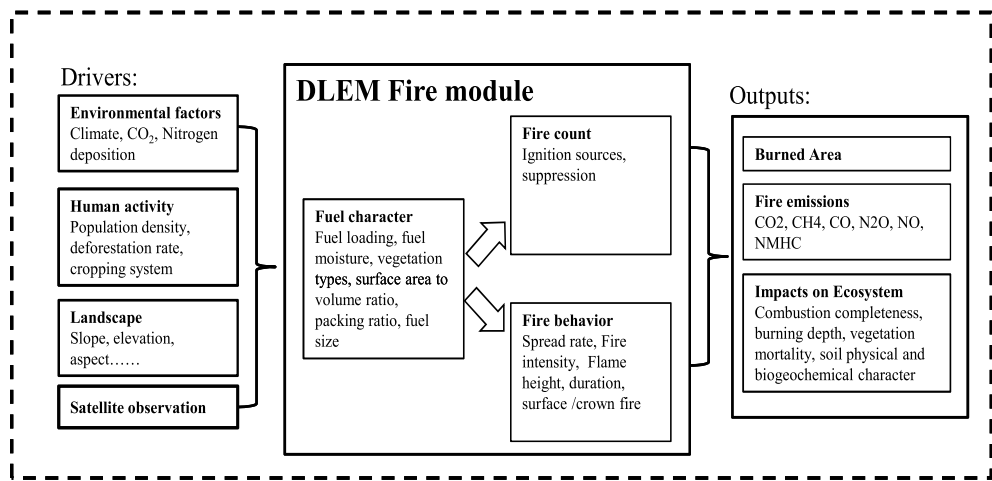


Figure 1. Conceptual diagram presenting inputs, outputs, and the major processes of DLEM-Fire.

burned area, fire emissions, and fire impacts on ecosystem function and structure by simulating fuel characteristics, number of fires, and fire behavior (Figure 1). Since this study aims to reconstruct the historical burned area, we focus on the algorithm of estimating burned area, rather than fire emissions and fire impacts. For each grid, the daily burned fraction BF is calculated as

$$BF = BF' \times v = (BF_{wd}' + BF_{def}' + BF_{ag}') \times v \quad (1)$$

where BF' is DLEM simulated burned fraction prior to coupling with satellite information, which is equal to the sum of DLEM simulated wildfire burned fraction (BF_{wd}'), deforestation fire burned fraction (BF_{def}'), and agricultural fire burned fraction (BF_{ag}'); and v is the grid-based satellite-adjusted scalar to regulate the magnitude and spatial distribution of fires and is calculated as the quotient of satellite-observed fire climatology and DLEM simulated fire climatology prior to coupling with satellite information. The detail process to estimate v can be found in section 2.3.

The following briefly describes the wildfire, agricultural fire, and deforestation fire schemes adapted from previous fire models [Arora and Boer, 2005; Pechony and Shindell, 2009; Li et al., 2012, 2013].

Daily burned fraction in each grid as a result of wildfire, BF_{wd}' (day^{-1}), is calculated as a function of the number of daily fire events, N_f (count d^{-1}), average burned area of each fire event, A_f ($\text{km}^2 \text{count}^{-1}$), and grid area, A_{grid} (km^2):

$$BF_{wd}' = N_f A_f / A_{\text{grid}} \quad (2)$$

The number of daily fire events, N_f (count d^{-1}), is expressed as

$$N_f = (I_a + I_n)(1 - f_s)(1 - f_{\text{crop}})P_m P_b A_{\text{grid}} \quad (3)$$

where I_a and I_n are the anthropogenic and natural ignition ($\text{count km}^{-2} \text{d}^{-1}$), respectively; f_s is the fraction of suppressed fires; f_{crop} is the fraction of cropland; P_m is reduction factor on ignition probability caused by fuel moisture; and P_b is the reduction factor on ignition probability caused by the insufficient fuel loading.

At the global level, cloud-to-ground lightning is the major natural fire ignition source. The natural ignition, I_n ($\text{count km}^{-2} \text{d}^{-1}$), is estimated through the frequency of lightning flashes, I_l ($\text{flash km}^{-2} \text{d}^{-1}$), and latitude, λ [Prentice and Mackerras, 1977]:

$$I_n = I_l [5.16 + 2.16 \cos(3\lambda)]^{-1} \quad (4)$$

Anthropogenic ignition, I_a ($\text{count km}^{-2} \text{d}^{-1}$), is parameterized as

$$I_a = P_D \alpha k(P_D) \quad (5)$$

where P_D is population density (person km^{-2}); α is the daily potential anthropogenic ignitions (1.3×10^{-4} , $\text{count person}^{-1} \text{d}^{-1}$); and $k(P_D)$ is a population density-related parameter for adjusting anthropogenic ignition potential ($= 6.8 P_D^{-0.6}$) [Venevsky et al., 2002].

Fire suppression, f_s , is estimated as a function of population density:

$$f_s = 0.99 - 0.98 \exp(-0.025P_D) \quad (6)$$

The reduction factor, P_m , is calculated as a function of the available soil water:

$$P_m = \begin{cases} 1, & \theta < \theta_{wp} \\ \exp\left[-\pi(\theta - \theta_{wp})^2 / (\theta_{fc} - \theta_{wp})^2\right], & \theta \geq \theta_{wp} \end{cases} \quad (7)$$

where θ is the volumetric soil water content in the top 20 cm; and θ_{wp} and θ_{fc} are the volumetric soil water content at wilting point and field capacity, respectively.

The reduction factor, P_b , is determined by the abundance of fuel loading and is calculated as a function of aboveground biomass [Arora and Boer, 2005]:

$$P_b = \begin{cases} 1, & b_{ag} > b_{up} \\ (b_{ag} - b_{low}) / (b_{up} - b_{low}), & b_{low} \leq b_{ag} \leq b_{up} \\ 0, & b_{ag} < b_{low} \end{cases} \quad (8)$$

where b_{ag} is the aboveground biomass (g C m^{-2}), including leaf, stem, woody debris, and litter; b_{up} is the upper limit of aboveground biomass (1000 g C m^{-2}) where fuel load is not a limiting factor; and b_{low} is the lower limit of aboveground biomass (150 g C m^{-2}), below which ignition probability is 0.

The post-fire area, i.e., fire spread from starting point, is postulated to be elliptical in shape. The equation to calculate burned area of single fire event is

$$A_f = 0.25\pi u_{\text{down}}^2 \tau^2 (1 + 1/H_B)^2 / L_B \quad (9)$$

where u_{down} is fire spread rate in downwind direction (km h^{-1}); τ is the fire duration (h); and L_B and H_B are the length-to-breadth ratio and head-to-back ratio of the post-fire area, respectively. Fire spread rate, u_{down} (km h^{-1}), is computed as

$$u_{\text{down}} = u_{\max} f_m f_{vpd} f_w \quad (10)$$

where u_{\max} is the maximum spread rate in optimum condition (0.6 km h^{-1}); and f_m , f_{vpd} , and f_w are the limiting scalars of fuel moisture, vapor pressure deficit (VPD), and wind speed to adjust spread rate, respectively. The fuel moisture scalar, f_m , is estimated as

$$f_m = \begin{cases} 1, & \theta < \theta_{wp} \\ (\theta_{sat} - \theta)^2 / (\theta_{sat} - \theta_{wp})^2, & \theta \geq \theta_{wp} \end{cases} \quad (11)$$

VPD scalar, f_{vpd} , is calculated as [Pechony and Shindell, 2009]

$$f_{vpd} = 20 \times 10^Z (1 - RH/100) \quad (12)$$

and

$$\begin{aligned} Z = & -7.90298(T_s/T - 1) + 5.02808 \cdot \log(T_s/T) - 1.3816 \times 10^{-7} (10^{11.344(1-T_s/T)} - 1) \\ & + 8.1328 \times 10^{-3} (10^{-3.49149(1-T_s/T)} - 1) \end{aligned} \quad (13)$$

where RH is relative humidity (%), T is air temperature (K), and T_s is water boiling point temperature (373.15 K).

Wind speed scalar, f_w , is parameterized as [Li et al., 2012]

$$f_w = 0.1L_B / (1 + 1/H_B) \quad (14)$$

Fire duration, τ (h), is the time that each fire lasts, which is estimated as a function of the global average fire persistence τ_{ave} (24 h) and the slope of landscape (γ):

$$\tau = \begin{cases} \tau_{\text{ave}}, & \gamma < \gamma_{\min} \\ \tau_{\text{ave}}(\gamma_{\max} - \gamma) / (\gamma_{\max} - \gamma_{\min}), & \gamma_{\min} \leq \gamma \leq \gamma_{\max} \\ 0, & \gamma > \gamma_{\max} \end{cases} \quad (15)$$

Table 1. The Input Data Sets for DLEM-Fire^a

Variables	Period	Sources
Climate	1901–2007	CRU/NCEP
Population density	1901–2005	HYDE3.1
Lightning frequency	climatology during 1995–2011	NASA LIS/OTD
GDP	2000	van Vuuren <i>et al.</i> [2007]
CO ₂	1901–2007	CDIAC
Land use/cover change	1901–2007	SYNMAP and Hurt et al. [2011]
Topography	Static	GTOPO30
Satellite-observed fire climatology	climatology during 1997–2007	GFED3

^aThe variables simulated by DLEM, such as soil moisture and fuel loading, are not included in this table.

where γ_{\min} (2°) and γ_{\max} (10°) are the lower and upper limits of the slope effect on fire duration, respectively. Terrain with steep slopes indicates more watercourse or rocks, which could break down fuel continuity and reduce fire persistence time [Pfeiffer and Kaplan, 2012].

Length-to-breadth ratio (L_B) and head-to-back ratio (H_B) are computed according to wind speed, w (m/s):

$$L_B = 1 + 10[1 - \exp(-0.06w)] \quad (16)$$

$$H_B = \left[L_B + (L_B^2 - 1)^{0.5} \right] / \left[L_B - (L_B^2 + 1)^{0.5} \right] \quad (17)$$

The burned area of agricultural fire, BF_{ag}' (month⁻¹), is calculated as

$$BF_{ag}' = 0.2f_{crop}f_{harv}P_bf_{GDP} \quad (18)$$

where f_{crop} is the fraction of cropland, f_{harv} is the monthly harvest index (1 means harvest happens, and 0 stands for no harvest happens), P_b is the reduction factor of fuel loading which is the same as that used for wildfire, and f_{GDP} is the socioeconomic factor indicated by gross domestic production (GDP), which is set by Li *et al.* [2013].

The burned area of deforestation fire, BF_{def}' (month⁻¹), is calculated as

$$BF_{def}' = f_{def}P_bf_{dry} \quad (19)$$

where f_{def} is the annual deforestation fraction of tropical forests, P_b is the same reduction factor of fuel loading as used for wildfires, and f_{dry} is monthly dryness function indicating the influence of dry season, which is computed by the ratio of monthly precipitation to potential evapotranspiration (P/PET)

$$f_{dry} = \begin{cases} 1 - P/PET, & P/PET < 1 \\ 0, & P/PET \geq 1 \end{cases} \quad (20)$$

2.2. Data Sets

Gridded ($0.5^\circ \times 0.5^\circ$), georeferenced data sets were compiled to drive DLEM-Fire, including satellite-observed fire climatology, climate (temperature, precipitation, relative humidity, wind speed, and lightning frequency), atmospheric CO₂ concentration, population density, nitrogen deposition, land use/cover change and land management practices (cropping system, fertilization and irrigation), GDP, and topography data (elevation, slope, and aspect) for the entire globe (Table 1). Satellite-observed fire climatology was derived from the GFED3 burned area from 1997 to 2007, which was developed based on multiple satellite sensors (Moderate Resolution Imaging Spectroradiometer (MODIS), Tropical Rainfall Measuring Mission (TRMM), Visible and Infrared Scanner (VIIRS), and Along Track Scanning Radiometer (ASTR)) [Giglio *et al.*, 2010]. Another satellite burned area product, MCD45A1 [Roy *et al.*, 2008], was used for validation. Daily climate variables (1901–2007) were generated based on Climatic Research Unit/National Centers for Environmental Prediction (CRU/NCEP) data set (http://nacp.ornl.gov/thredds/fileServer/reccapDriver/cru_ncep/analysis/readme.htm). Daily lightning frequency was collected from NASA Lightning Imaging Sensor/Optical Transient Detector (LIS/OTD) (<ftp://ghrc.nsstc.nasa.gov/pub/lis/climatology/HRACT/>), which is the climatology of daily lightning frequency for the period 1995–2011. Due to the lack of historical lightning data, the 17 year climatology was applied to each year across the study period. Population density (1901–2005) was extracted from the History Database of the Global Environment (HYDE3.1) [Goldewijk *et al.*, 2010] and assumed unchanged since 2005 due to the lack of data in 2006 and 2007. The CO₂ concentration was obtained from the Carbon Dioxide Information Analysis Center (CDIAC). Land use/cover change was developed based on Synergetic Land Cover Product

Table 2. Experimental Design for This Study^a

Simulation	Scenario	Climate	LCLUC and Population	CO ₂ and Ndep
sim0	Baseline	1901	1901	1901
sim1	All-Combined	1901–2007	1901–2005 (L), 1901–2007 (P)	1901–2007
sim2	Climate only	1901–2007	1901	1901
sim3	Human only	1901	1901–2005 (L), 1901–2007 (P)	1901
sim4	CO ₂ + Ndep	1901	1901	1901–2007

^aLCLUC, land cover and land use change; Ndep, nitrogen deposition; 1901–2007 indicates the data set in 1901–2007 was used to drive model; 1901 indicates the data set in 1901 was used to drive model through the whole simulation period; 1901–2005 (L), 1901–2007 (P) indicates LCLUC data ends at 2005 and population data ends at 2007.

(SYNMAP) [Jung *et al.*, 2006] and land use conversion data [Hurt et al., 2011]. Annual deforestation rate was computed through the expansion of cropland and pasture within the grid where forest exists. Cropping system and crop phenology were identified based on a global crop geographic distribution map [Leff *et al.*, 2004] and MODIS Leaf Area Index (LAI) products. Gross domestic production (GDP) data set in 2000 is from van Vuuren *et al.* [2007]. Elevation, slope, and aspect were derived from Global 30 Arc-Second Elevation product (<https://lta.cr.usgs.gov/GTOPO30>).

2.3. Model Implementation and Experimental Design

DLEM-Fire implementation is composed of three stages: (1) equilibrium run, (2) spin-up, and (3) transient run. The equilibrium run aims to determine the initial condition on 1 January 1901. In the equilibrium run, the model is fed with detrended climate data from 1901 to 1930 and atmospheric composition and land cover/use pattern in 1901 to reach an equilibrium state for carbon, nitrogen, and water (i.e., the changes in annual carbon, nitrogen, and water fluxes and pools are less than 0.1 g C m⁻², 0.1 g N m⁻², and 0.1 mm among consecutive years). After equilibrium state was reached, the model was run another 100 years for spin-up. In the transient mode, DLEM-Fire was driven by the time series of all input data sets and had two-type simulations: Type I was run without integrating satellite information, in which the annual satellite-adjusted scalar (v) on each grid was estimated as the quotient of the average annual burned area of GFED3 and DLEM-Fire simulated average annual burned area from 1997 to 2007; type II was run after type I simulation by coupling the satellite-adjusted scalar (v) estimated through type I simulation, and all the experiments below were based on type II simulation.

Five experiments were designed to estimate the global burned area and quantify the relative contribution of human activities, climate change, and atmospheric components (CO₂ and nitrogen deposition), respectively (Table 2). In the “baseline” scenario (sim0), all the forcing data sets were kept at the level in 1901 to estimate the inherent model fluctuation. The “all-Combined” scenario (sim1) considered the historical variation of all the driven factors. The “climate only” scenario (sim2) was driven by historical climate condition but constant human activities, CO₂ concentration, and nitrogen deposition. The “human only” scenario (sim3) was forced by dynamic human activities but static climate, CO₂ concentration, and nitrogen deposition. The “CO₂ + Ndep” scenario (sim4) was forced by historical CO₂ concentration and nitrogen deposition but static climate and human activities.

2.4. Model Evaluation

The cross-validation scheme was used to evaluate DLEM-Fire simulated global fire patterns according to two satellite-based global fire products (GFED3 and MCD45A1). The DLEM-Fire simulation and GFED3 have 11 years overlap from 1997 to 2007. In the evaluation, 10 years from 11 overlapped years are selected to construct the satellite-adjusted scalar (v). And then the scalar was applied to estimate burned area of the left year to compare with GFED3 observation. This procedure was rotated 11 times to make every overlapped year to be selected.

2.4.1. Evaluation of Global Fire Distribution

The global fire distribution from 2002 to 2007 simulated by DLEM-Fire was compared with GFED3 and MCD45A1 data (Figure 2). The DLEM-Fire simulated tropical burned area was ~2% higher than GFED3 and ~4% higher than MCD45A1; DLEM-Fire simulated burned area in northern high latitudes was ~24.9% lower than GFED3 and ~11.7% higher than MCD45A1; DLEM-Fire simulated burned area in northern extratropics was ~9.5% lower than GFED3 and ~24.4% lower than MCD45A1; DLEM-Fire simulated burned area in southern extratropics was

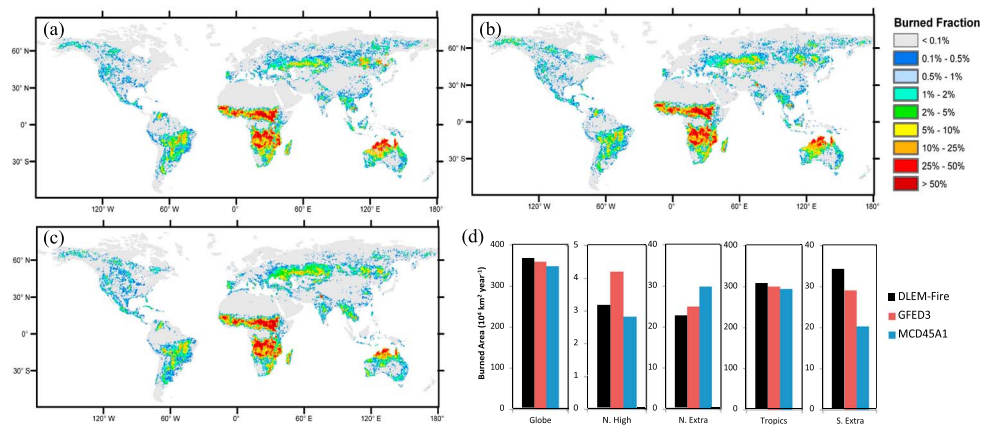


Figure 2. Six-year average of global burned fraction from 2002 to 2007 estimated by (a) DLEM-Fire, (b) GFED3, and (c) MCD45A1, and (d) the comparison of global and regional burned area in N. High, northern high latitudes ($>55^\circ\text{N}$); N. Extra, northern extratropics (55°N to 30°N); Tropics (30°N to 20°S); S. Extra, southern extratropics ($>20^\circ\text{S}$)

~17.2% higher than GFED3 and ~68.1% higher than MCD45A1 (Figure 2d). Spatial correlations of the 6 year average burned area between our study and the two satellite products were 0.96 and 0.91, respectively. The result indicated the spatial patterns of DLEM-Fire simulation agreed with GFED3 and MCD45A1. Li et al. [2013] tested three fire schemes coupled in the Community Land Model (CLM) and reported the spatial correlations between three simulated global burned areas and GFED3 were 0.23, 0.44, and 0.69, respectively. The higher spatial correlations in our study suggested that our method by incorporating remote sensing data could substantially improve the accuracy of simulated fire spatial pattern.

2.4.2. Evaluation of Interannual Variations

Interannual variation from 1997 to 2007 of the global burned area from the DLEM-Fire simulation was compared with GFED3, MCD45A1, and Mouillet and Field [2005] (Figure 3). DLEM-Fire estimated global burned area as $369.4 \times 10^4 \text{ km}^2 \text{ yr}^{-1}$ compared to $374.9 \times 10^4 \text{ km}^2 \text{ yr}^{-1}$ estimated by GFED3. During 2002–2007, MCD45A1 estimated an area of $347.9 \times 10^4 \text{ km}^2 \text{ yr}^{-1}$, while we estimated $366.6 \times 10^4 \text{ km}^2 \text{ yr}^{-1}$. In terms of interannual variation, our estimation also presented a similar pattern as GFED3 and MCD45A1. From 1997 to 2000, the annual mean global burned area estimated by Mouillet and Field [2005] was $602 \times 10^4 \text{ km}^2 \text{ yr}^{-1}$. Their estimate was 61% higher than our estimation and 51.3% higher than GFED3. This comparison with satellite products demonstrated that our estimates for the global burned area and temporal patterns were close to satellite observations.

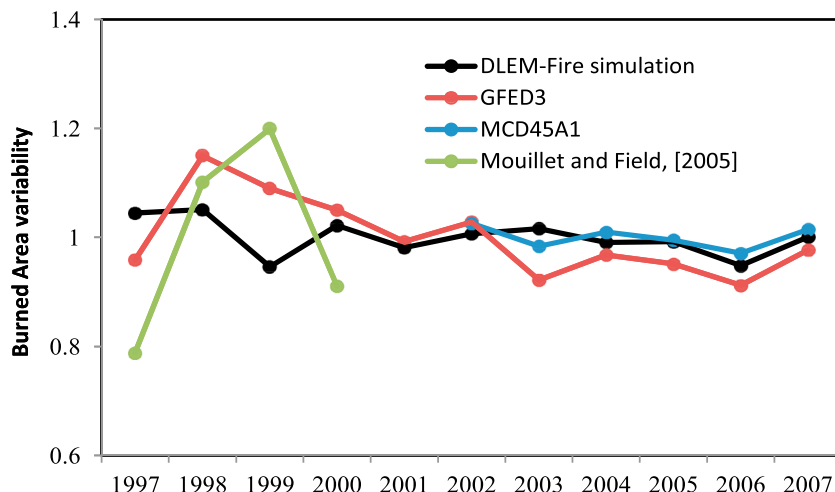


Figure 3. Interannual variations of global burned area (annual burned area normalized by mean) estimated from multiple global burned area products.

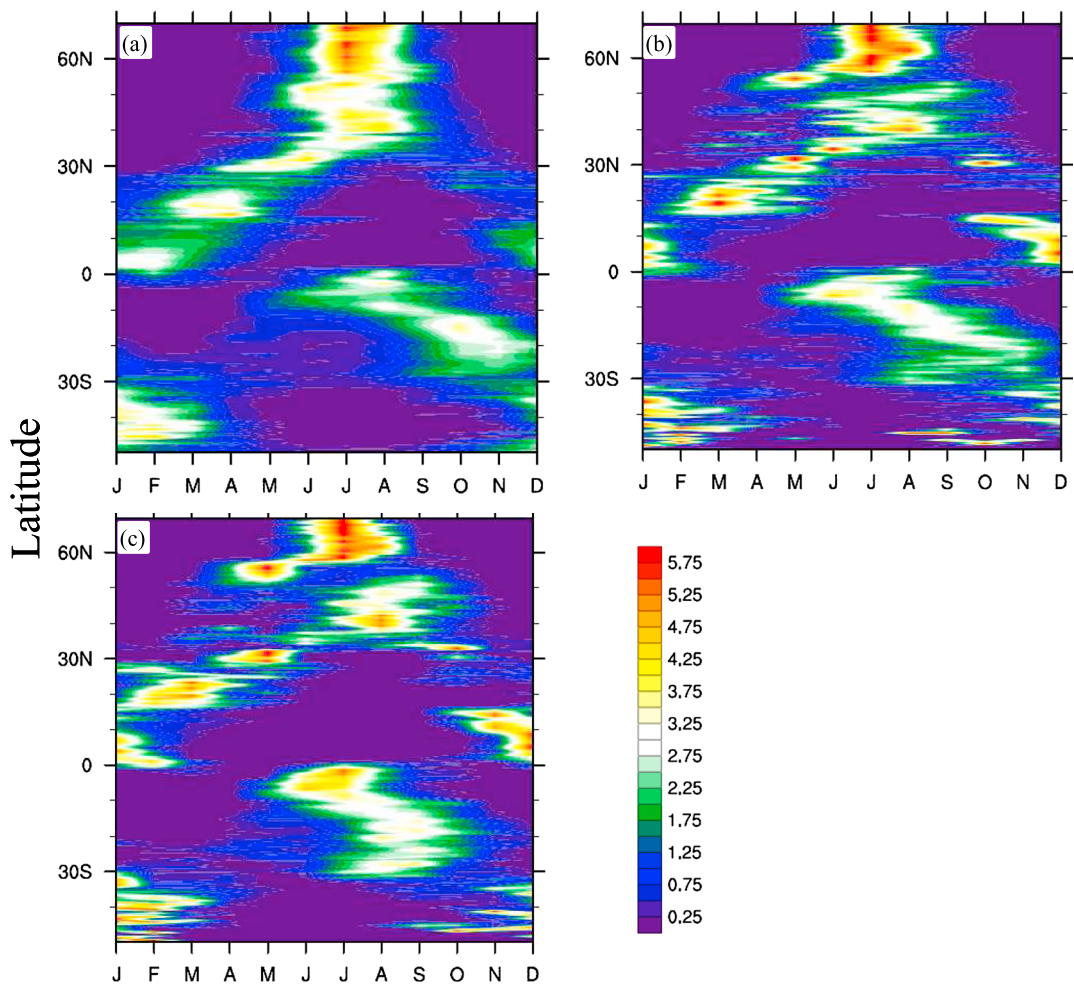


Figure 4. The zonal mean of monthly burned area of 6 year average (2002–2007), as normalized by the monthly average burned area of that latitude. (a) DLEM-Fire simulation, (b) GFED3, and (c) MCD45A1.

2.4.3. Evaluation of Fire Seasonality

Fire seasonality simulated by DLEM-Fire from 2002 to 2007 was compared with GFED3 and MCD45A1 products along latitude (Figure 4). All data sets demonstrated evident seasonal fire variation. At the middle and high latitudes, 40°N to 70°N, GFED3 and MCD45A1 revealed fires were likely to happen from June to September. Our simulated fire season was similar to GFED3 and MCD45A1, which also spanned from June to September. The fire season in summer was probably caused by the relatively warm climate, which dried up fuel moisture and increased fire danger potential. From 15°N to 40°N, GFED3 and MCD45A1 displayed fire season lasted from February to June, and the peak fire month shifted gradually from summer to spring toward the equator, roughly at a rate of 3.6 days per latitude degree. Our simulation also showed spring fire season shifting from June to February as it moved toward the equator. Overall, all data sets indicated fires were scarce in summer, which could be attributed to summer precipitation dampening fuel and reducing fire risk. From 15°N to the equator, satellite products revealed the fire season lasted from November to January, while the fire season of DLEM-Fire simulation was from December to March. In Southern Hemisphere from equator to 10°S, high fire activities in June and July were detected by all the data sets. From 10°S to 30°S, GFED3 and DLEM-Fire simulation demonstrated a fire peak from September to November, while MCD45A1 indicated fires were more active in August and September. From 30°S to 50°S, the fires estimated by GFED3, MCD45A1, and DLEM-Fire simulation were concentrated in December, January, and February. In general, our estimated seasonal variation was similar to GFED3 and MCD45A1.

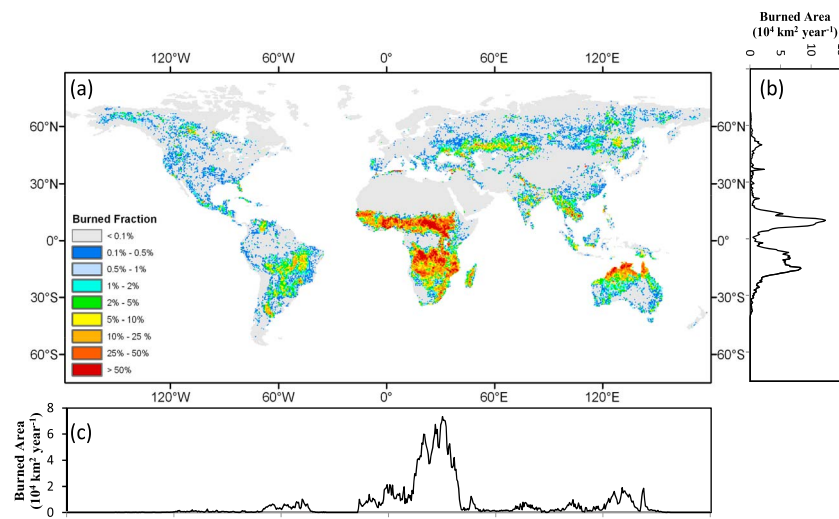


Figure 5. Spatial distribution of global fire. (a) Average burned fraction from 1901 to 2007, (b) zonal sum of burned area per 0.5° latitude, and (c) meridional sum of burned area per 0.5° longitude.

3. Results and Discussions

3.1. Spatial Patterns

During 1901–2007, our simulated global average burned area was $442.1 \times 10^4 \text{ km}^2 \text{ yr}^{-1}$, of which approximately 70.2% and 10.1% occurred in Africa and Oceania, respectively (Figure 5). The regions with high burned fraction included Africa, Northern Australia, and South America, where fuel was sufficient and dry season was long enough; the regions with low burned fraction were distributed in cold areas (e.g., Tibet plateau), very humid areas (e.g., interior Amazon rainforest), and regions with low fuel loading (e.g., Sahara desert) (Figure 5a). In the west-east direction, maximum burned area occurred between 10°E and 40°E, which was mainly due to fire in Africa (Figure 5c). In the north-south direction, two high burned area zones were shown clearly: One was approximately located at 10°N, and the other one was within 5°S–20°S (Figure 5b).

Table 3 lists global burned area estimated by satellite observations, process-based fire models, and hybrid methods. Satellite observations (GFED, MCD45A1, L3JRC, GBA2000, and GlobScar) clustered the burned area around $350 \times 10^4 \text{ km}^2 \text{ yr}^{-1}$ in the 2000s. Yet Randerson *et al.* [2012] argued that satellite imagery with coarse spatial resolution failed to detect small fires and global burned area could be more than $400 \times 10^4 \text{ km}^2 \text{ yr}^{-1}$. Fire models estimated a similar global burned area as satellite observations, since satellite observed fires were often used as benchmarks to calibrated fire models [Kelley *et al.*, 2012]. Annual burned areas from 1997 to 2004 estimated by Kloster *et al.* [2010] and Li *et al.* [2012] were $300 \times 10^4 \text{ km}^2$ and $330 \times 10^4 \text{ km}^2$, respectively. Our estimated global burned area was $362.6 \times 10^4 \text{ km}^2 \text{ yr}^{-1}$ in the 2000s, which fell within the range of satellite observations.

3.2. Temporal Variations

For the period from 1901 to 2007, Mann-Kendall trend test indicated a significant decreasing trend in global burned area at the rate of $1.28 \times 10^4 \text{ km}^2 \text{ yr}^{-1}$, with a relatively small annual variation ($CV = 0.1$) (Table 4). The largest burned area was in 1912 ($552.1 \times 10^4 \text{ km}^2$), and the lowest burned area appeared in 2006 ($348.9 \times 10^4 \text{ km}^2$). Decadal burned area from the 1900s through the 2000s (2000s in this study refers to 2001–2007) varied between $362.6 \times 10^4 \text{ km}^2 \text{ yr}^{-1}$ and $492.3 \times 10^4 \text{ km}^2 \text{ yr}^{-1}$ (Figure 6). The burned area in the tropics and extratropics presented a significant declining trend, while no significant trend was detected at high latitudes.

The estimation of our study suggesting global fires declined in the twentieth century was supported by Antarctic ice core record of atmospheric carbon monoxide of Wang *et al.* [2010], charcoal records of Marlon *et al.* [2008], and fire model simulation of Li *et al.* [2013]. Prentice [2010] argued present biomass burning is at a historical low because of human-induced fuel loads reduction and fuel beds fragmentation. However, there are some studies presenting a different trend. As revealed by the data set of Mouillot and Field [2005], $503 \times 10^4 \text{ km}^2$ of land area experienced fire annually in the twentieth century, with an upward trend after the

Table 3. Annual Global Burned Area Estimated by Different Studies

Source	Study Period	Annual Burned Area ($10^4 \text{ km}^2 \text{ yr}^{-1}$)	Study Approach
GFED4 [Giglio et al., 2013]	1997–2011	348	multiple satellite observations
GFED3 [Giglio et al., 2010]	1997–2010	363	multiple satellite observations
GFED2 [van der Werf et al., 2006]	1997–2004	329	multiple satellite observations
MCD45A1 [Roy et al., 2008]	2002–2010	338	satellite observation
L3JRC [Tansey et al., 2008]	2000–2007	392	satellite observation
GBA2000 [Tansey et al., 2004]	2000	350	satellite observation
GlobScar [Simon et al., 2004]	2000	211	satellite observation
[Randerson et al., 2012]	2001–2010	464	satellite observation
[Kloster et al., 2010]	1997–2004	300	process-based fire model
[Li et al., 2012]	1997–2004	330	process-based fire model
[Schultz et al., 2008]	1960–2000	383	hybrid of official statistics and process-based fire model
[Mouillot and Field, 2005]	1900–2000	503	hybrid official statistics and satellite observation
This study	1901–2007	442	hybrid of process-based fire model and satellite observation

1950s. However, their data set should be used with caution, since they made some assumptions and interpolations to quantify the burned area based on the scattered and qualitative fire records, which may bring in large uncertainties. Besides that, their data set may not be able to reflect the variation of burned area as influenced by driving forces, as they disregarded the underlying mechanism of fire activities. *van der Werf et al.* [2013] analyzed biomass burning sources and historical methane record and argued that the historical high levels of biomass burning implied by ice core record of carbon monoxide are likely overestimated. Yet ambient methane concentration may not be a good indicator of biomass burning, because methane emission from fires only contributes 5.6% of global emission [Kirschke et al., 2013] and explains only 15% of global emission anomalies, as compared with 70% explained by wetland emissions [Bousquet et al., 2006]. *Kloster et al.* [2010] simulated global burned area and found a downward trend from the 1900s to the 1960s, followed by an upward trend from the 1970s to the 1990s. The simulation of *Pechony and Shindell* [2010] showed global fire activity increases from the 1900s to the 1940s and then decreases afterward. These simulations contradict our estimated trend, which may be attributed to the different parameterization of anthropogenic impact on fire.

3.3. Relative Contribution of Human Activities, Climate, and Atmospheric Components

Previous studies have reported the impacts of climate or human activities on fire regime, while few of them quantified the relative contribution of multiple factors. The impact of atmospheric components, such as CO₂ and nitrogen deposition, was basically neglected. In this study, we conducted factorial experiments to quantify the relative contribution of human activities and multiple environmental factors from 1901 to 2007. The contribution of climate on burned area was estimated by the difference between sim2 and sim0; the contribution of human activity was estimated by the difference between sim3 and sim0; and the contribution of CO₂ and nitrogen deposition was estimated by the difference between sim4 and sim0 (see experimental design in section 2.3).

3.3.1. Human Activities

Anthropogenic impacts are critical factors in determining global fire patterns, since they may increase or decrease wildfire activity through grazing, clearing forests, altering ignition patterns, and suppressing fires [Bowman et al., 2011]. *Marlon et al.* [2008] found an abrupt fire reduction after the 1870s in the tropics and extratropics as a response to cropland and pasture expansion. The model simulation of *Pechony and Shindell* [2010] suggested global fire is an anthropogenic-driven phenomenon in the twentieth century. In our study,

Table 4. The Mean, CV, and Trend of Global and Regional Burned Areas During 1901–2007^a

	Mean ($10^4 \text{ km}^2 \text{ yr}^{-1}$)	CV	Slope ($10^4 \text{ km}^2 \text{ yr}^{-1}$)	Trend Significance
Global	442.1	0.1	-1.28 (-0.29%)	S
N. High	4.7	0.43	-0.01 (-0.21%)	NS
N. Extra	30.4	0.43	-0.37 (-1.21%)	S
Tropics	374.7	0.09	-0.84 (-0.22%)	S
S. Extra	32.3	0.14	-0.05 (-0.15%)	S

^aTrends were analyzed with significance of Mann-Kendall test (S for significant, $p < 0.05$; NS for not significant, $p \geq 0.05$) and Sen's slope; CV, coefficient of variation; in the column of "Slope," the values within the parentheses are relative slope (slope normalized by the average burned area).

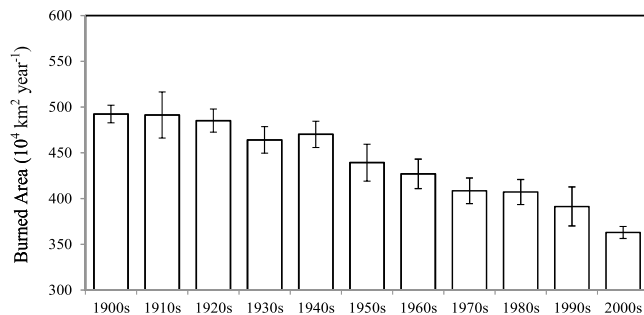


Figure 6. Decadal variation of global burned area. Error bar refers to the standard deviation of annual burned area within that decade.

human activities remarkably reduced burned area in the tropics as a whole region (Figure 7d), which is mainly contributed by the fire reduction in the tropical Africa and tropical Asia. In northern extratropics, human impact continuously increased from 1900s to 1980s (Figure 7c). Until the 1980s, burned area was reduced by $31.7 \times 10^4 \text{ km}^2 \text{ yr}^{-1}$ compared to the beginning of the twentieth century, in which human activities contributed $23.6 \times 10^4 \text{ km}^2 \text{ yr}^{-1}$. Studies have attributed the reduction of large fires in United States during this period to extensive livestock grazing and fire suppression efforts [Belsky and Blumenthal, 1997; Savage and Swetnam, 1990]. Fire models also suggested fire suppression efforts have substantially reduced the extent of wildfire in United States [Lenihan et al., 2008]. In China, burned area showed a downward trend from the 1950s to the 1990s. From 1981, fire suppression was strengthened across the forested region and abruptly reduced burned area [Lü et al., 2006]. At high latitudes, our results indicate human impact was relatively small compared with climate effects (Figure 7b), although fire suppression was an important component in forest management [Flannigan et al., 2005]. Generally, in the twentieth century, human activities acted as the dominant factor in determining the downward trend in the tropics and extratropics, but its impact was relatively minor at high latitudes.

3.3.2. Climate Variation

At high latitudes, we found fire temporal pattern was closely related to climate variation (Figure 7b). The contribution of climate variation to the burned area ($\text{sim2} - \text{sim0}$) dropped down from $2.3 \times 10^4 \text{ km}^2 \text{ yr}^{-1}$ to $-0.5 \times 10^4 \text{ km}^2 \text{ yr}^{-1}$ during the 1930s–1960s and increased from $-0.5 \times 10^4 \text{ km}^2 \text{ yr}^{-1}$ to $3.41 \times 10^4 \text{ km}^2 \text{ yr}^{-1}$ during the 1960s–1990s. Correspondingly, the burned area decreased by $2.8 \times 10^4 \text{ km}^2 \text{ yr}^{-1}$ from the 1930s to 1960s and increased by $3 \times 10^4 \text{ km}^2 \text{ yr}^{-1}$ from the 1960s to 1990s, which indicated decadal variation of burned area at high latitudes was controlled by climate variation. Our estimated temporal pattern of burned area was comparable with other studies. The Large Fire Database, which includes large fire information in Canada starting from 1959 [Stocks et al., 2002], indicated an upward trend in the amount of area burned in Canada from 1959 to the end of the twentieth century. Wagner [1988] described burned area in Canada as a downward trend from the 1940s to the 1960s, followed by an upward trend from the 1960s to the 1990s. Krezek-Hanes et al. [2011] reported Canada burned area increased from the 1960s to the 1990s and then decreased in the 2000s. Flannigan et al. [2005] suggested fire regimes in Canada were controlled by climate factors with temperature as the most important predictor to estimate burned area.

In the extratropics, climate influence was also important for fire activities. In the western United States, wildfire frequency has increased since the mid-1980s in response to the climate warming and extended fire season [Westerling et al., 2006]. As demonstrated by Figure 7c, our simulation captured the upward trend of burned area in northern extratropics from the 1980s to the 2000s. Within this period, climate dominated the fire trend, and its contribution increased from $-7.1 \times 10^4 \text{ km}^2 \text{ yr}^{-1}$ to $7.8 \times 10^4 \text{ km}^2 \text{ yr}^{-1}$. In southern Africa, either human activities or climate change could act as the primary factor in shaping fire regimes [Archibald et al., 2009]. As shown in Figure 7e, both climate and human activities were critical in southern extratropics. Although human impact was identified as the dominant factor in the extratropics, its influence was largely counteracted by climate change. If the warming trend continues in the 21st century, climate impact may outweigh anthropogenic influence and become the primary factor in the extratropics. In general, climate variation was the primacy of fire variation at high latitudes and is becoming increasingly important in extratropics in the context of global warming. However, the impact of climate variation was much less than anthropogenic influences in tropical regions and at the global level in the twentieth century.

human impact was identified as the primary factor accounting for the declining trend in global fire activity, which reduced global burned area by $141.2 \times 10^4 \text{ km}^2 \text{ yr}^{-1}$ in the 2000s ($\text{sim3} - \text{sim0}$) (Figure 7a). In the tropics, cropland area increased by 76.6%, and population increased by 310% from the 1900s to 2000s.

Although it has been reported that deforestation rate and burned area in Amazonia increased substantially since the 1970s [Houghton et al., 2000],

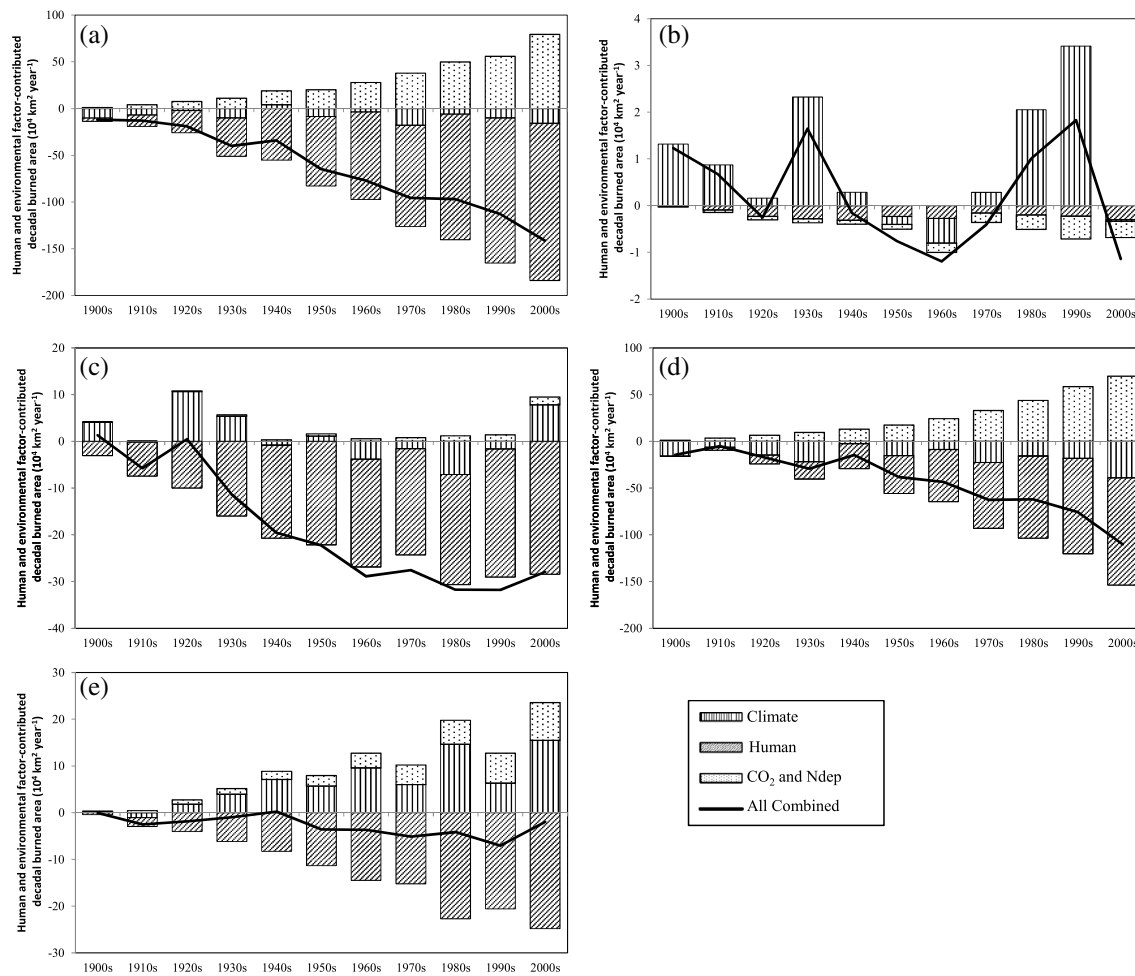


Figure 7. Factorial contributions to the inter-decadal variation of burned area. (a) Globe, (b) northern high latitudes ($>55^\circ\text{N}$), (c) northern extratropics (55°N to 30°N), (d) tropics (30°N to 20°S), and (e) southern extratropics ($>20^\circ\text{S}$).

3.3.3. Atmospheric Components

The impacts of atmospheric components on fire activity are rarely studied, because they are often covered up by the impacts of climate and human activities and their effect is difficult to detect based on short-term fire observations. The impacts of atmospheric components on ecological and hydrological processes have been verified by observations and model simulations. Theoretically, CO₂ and nitrogen deposition can stimulate fire activities by boosting ecosystem productivity, vegetation biomass, and then fuel loading [Norby *et al.*, 2010; Thomas *et al.*, 2009]; at the same time, CO₂ can suppress fire occurrence by retaining more water in the soil [Nelson *et al.*, 2004] through reducing transpiration [Ainsworth and Rogers, 2007]. Fire models are able to provide insight into the impact of atmospheric components on burned area (sim4 – sim0). As indicated by our simulations, the impact of atmospheric components reduced burned area at high latitudes (Figure 7b). In the tropics and southern extratropics, elevated CO₂ and nitrogen deposition significantly stimulated fire activity (Figures 7d and 7e). In northern extratropics, the impact of elevated CO₂ and nitrogen deposition was small, which is probably because the positive effect and negative effect counteracted each other. At the global level, the impact of CO₂ and nitrogen deposition enhanced the burned area significantly (Figure 7a). Therefore, it is reasonable to expect that atmospheric components would have more significant effect on global fire regimes with the continuous increasing trend in CO₂ and nitrogen deposition projected in the 21st century [Lamarque *et al.*, 2005].

3.4. Uncertainties and Future Needs

The global burned area data set of this study agrees well with satellite fire products in terms of spatial and temporal patterns, but there should be some uncertainties when interpreting the results due to the input

data and fire model parameterization. The constant lightning frequency applied to each year in the study period was one source of uncertainties. Currently, the dynamic lightning data set prior to 1995 is still unavailable. To improve the spatial pattern of burned area simulation, GFED3 observed was integrated into DLEM-Fire. Thus, the reconstructed database has inherited uncertainties from GFED3 [Giglio *et al.*, 2010]. Fire activities are a complicated phenomenon depending on numerous parameters [Pechony and Shindell, 2009]. Although DLEM-Fire has addressed most critical factors influencing fire activity, some processes, such as the impact of fuel quality, have not been well represented in the current fire module. The parameterization of fire duration in the present study only considered average fire duration and natural fire breaks, which may lead to underestimate burned area caused by megafire events that last much longer than the average fire duration. A new algorithm estimating fire duration based on fuel characteristics, fire suppression effort, and weather conditions is expected to greatly improve model performance in estimating burned area under extreme climate conditions. On the deforested land in Amazonia, trees were reburned several times within 1 year to clear the land, and the burned area is at least twice the deforested area [Nepstad *et al.*, 1999]. Combustion completeness and climate conditions are the two major factors determining the burning times. DLEM-Fire probably underestimated the burned area of deforestation fire. Moreover, the performance of DLEM-Fire needs further evaluation as one component within the framework of DLEM. The information collected from field observations related to fuel loading, fuel consumption, fire emissions, and fire damage to vegetation would be valuable for model development, validation, and application.

4. Conclusions

In this study, we reconstructed a $0.5^\circ \times 0.5^\circ$ data set of the global burned area for the 20th and early 21st centuries based on a process-based fire model and made comparisons to satellite observations. The comparisons indicated our reconstructed global fire history was capable of capturing the spatial and temporal patterns of global fire activities. As indicated by this data set, the global burned area during 1901–2007 was $442.1 \times 10^4 \text{ km}^2 \text{ yr}^{-1}$ and showed a significant declining trend at the rate of $1.28 \times 10^4 \text{ km}^2 \text{ yr}^{-1}$. At the regional level, burned area in tropics and extratropics exhibited a significant declining trend, with no significant trend at high latitudes.

This study highlighted the evaluation of the relative contributions of human activities, climate, and atmospheric components to global and regional burned areas and was the first attempt to address the importance of elevated CO₂ and nitrogen deposition to fire regimes. The factorial experiments identified human activities as the dominant factor in determining the declining trend of burned area in the tropics and extratropics, and climate variation as the primary factor in shaping the decadal variation of burned area at high latitudes. The impact of climate change in extratropics is becoming increasingly important and may induce more fires in the context of global warming. Elevated CO₂ and nitrogen deposition enhanced burned area in tropics and southern extratropics but suppressed fire occurrence at high latitudes. The spatial and temporal information on global burned area derived from this study can be used for ecosystem, hydrological, and climate modeling as well as by policy makers for understanding and assessing complex interactions among fire, climate, and human in a changing global environment.

Acknowledgments

This research has been supported by NSF/USDA/DOE Decadal and Regional Climate Prediction using Earth System Models (AGS-1243220 and NIFC2013-35100-20516), USDA/USDI Joint Fire Science Program (JFSP 11172), NSF Dynamics of Coupled Natural and Human Systems (1210360), and NSF Computer and Network Systems (CNS-1059376).

References

- Ainsworth, E. A., and A. Rogers (2007), The response of photosynthesis and stomatal conductance to rising [CO₂]: Mechanisms and environmental interactions, *Plant Cell Environ.*, 30(3), 258–270.
- Andreae, M. (1991), Biomass burning—Its history, use, and distribution and its impact on environmental quality and global climate, *Global Biomass Burning—Atmospheric, Climatic, and Biospheric Implications*(A 92-37626 15-42), pp. 3–21, MIT Press Cambridge, MA.
- Archibald, S., D. P. Roy, V. Wilgen, W. Brian, and R. J. Scholes (2009), What limits fire? An examination of drivers of burnt area in Southern Africa, *Global Change Biol.*, 15(3), 613–630.
- Arora, V. K., and G. J. Boer (2005), Fire as an interactive component of dynamic vegetation models, *J. Geophys. Res.*, 110, G02008, doi:10.1029/2005JG000042.
- Baisan, C. H., and T. W. Swetnam (1990), Fire history on a desert mountain range: Rincon Mountain Wilderness, Arizona, USA, *Can. J. For. Res.*, 20(10), 1559–1569.
- Baker, W. L., and D. Ehle (2001), Uncertainty in surface-fire history: The case of ponderosa pine forests in the western United States, *Can. J. For. Res.*, 31(7), 1205–1226.
- Belsky, A. J., and D. M. Blumenthal (1997), Effects of livestock grazing on stand dynamics and soils in upland forests of the Interior West, *Conservation Biol.*, 11(2), 315–327.
- Bousquet, P., P. Ciais, J. Miller, E. Dlugokencky, D. Hauglustaine, C. Prigent, G. Van der Werf, P. Peylin, E.-G. Brunke, and C. Carouge (2006), Contribution of anthropogenic and natural sources to atmospheric methane variability, *Nature*, 443(7110), 439–443.
- Bowman, D. M., J. K. Balch, P. Artaxo, W. J. Bond, J. M. Carlson, M. A. Cochrane, C. M. D'Antonio, R. S. DeFries, J. C. Doyle, and S. P. Harrison (2009), Fire in the Earth system, *Science*, 324(5926), 481–484.

- Bowman, D. M., J. Balch, P. Artaxo, W. J. Bond, M. A. Cochrane, C. M. D'Antonio, R. DeFries, F. H. Johnston, J. E. Keeley, and M. A. Krawchuk (2011), The human dimension of fire regimes on Earth, *J. Biogeogr.*, 38(12), 2223–2236.
- Chen, G., H. Tian, C. Zhang, M. Liu, W. Ren, W. Zhu, A. H. Chappelka, S. A. Prior, and G. B. Lockaby (2012), Drought in the southern United States over the 20th century: Variability and its impacts on terrestrial ecosystem productivity and carbon storage, *Clim. Change*, 114(2), 379–397.
- Eidenshink, J., B. Schwind, K. Brewer, Z.-L. Zhu, B. Quayle, and S. Howard (2007), A project for monitoring trends in burn severity, *J. Assoc. Fire Ecol.*, 3(01), 3.
- Flannigan, M., K. Logan, B. Amiro, W. Skinner, and B. Stocks (2005), Future area burned in Canada, *Clim. change*, 72(1-2), 1–16.
- Flannigan, M., M. A. Krawchuk, W. J. de Groot, B. M. Wotton, and L. M. Gowman (2009), Implications of changing climate for global wildland fire, *Int. J. Wildland Fire*, 18(5), 483–507.
- Giglio, L., J. Randerson, G. Werf, P. Kasibhatla, G. Collatz, D. Morton, and R. DeFries (2010), Assessing variability and long-term trends in burned area by merging multiple satellite fire products, *Biogeosciences*, 7(3), 1171–1186.
- Giglio, L., J. T. Randerson, and G. R. van der Werf (2013), Analysis of daily, monthly, and annual burned area using the fourth-generation global fire emissions database (GFED4), *J. Geophys. Res. Biogeosci.*, 118, 317–328, doi:10.1002/jgrg.20042.
- Goldewijk, K. A., A. Beusen, and P. Janssen (2010), Long-term dynamic modeling of global population and built-up area in a spatially explicit way: HYDE 3.1, *The Holocene*, 20(4), 565–573.
- Grégoire, J.-M., K. Tansey, and J. Silva (2003), The GBA2000 initiative: Developing a global burnt area database from SPOT-VEGETATION imagery, *Int. J. Remote Sens.*, 24(6), 1369–1376.
- Houghton, R., D. Skole, C. A. Nobre, J. Hackler, K. Lawrence, and W. H. Chomentowski (2000), Annual fluxes of carbon from deforestation and regrowth in the Brazilian Amazon, *Nature*, 403(6767), 301–304.
- Hurtt, G., L. P. Chini, S. Frolking, R. Betts, J. Feddema, G. Fischer, J. Fisk, K. Hibbard, R. Houghton, and A. Janetos (2011), Harmonization of land-use scenarios for the period 1500–2100: 600 years of global gridded annual land-use transitions, wood harvest, and resulting secondary lands, *Clim. Change*, 109(1-2), 117–161.
- Jung, M., K. Henkel, M. Herold, and G. Churkina (2006), Exploiting synergies of global land cover products for carbon cycle modeling, *Remote Sens. Environ.*, 101(4), 534–553.
- Kelley, D. I., I. Colin Prentice, S. P. Harrison, H. Wang, M. Simard, J. B. Fisher, and K. O. Willis (2012), A comprehensive benchmarking system for evaluating global vegetation models, *Biogeosci. Discuss.*, 9(11), 15,723–15,785.
- Kirschke, S., P. Bousquet, P. Ciais, M. Saunois, J. G. Canadell, E. J. Dlugokencky, P. Bergamaschi, D. Bergmann, D. R. Blake, and L. Bruhwiler (2013), Three decades of global methane sources and sinks, *Nat. Geosci.*, 6(10), 813–823.
- Kitzberger, T., P. M. Brown, E. K. Heyerdahl, T. W. Swetnam, and T. T. Veblen (2007), Contingent Pacific–Atlantic Ocean influence on multi-century wildfire synchrony over western North America, *Proc. Natl. Acad. Sci. U. S. A.*, 104(2), 543–548.
- Kloster, S., N. M. Mahowald, J. T. Randerson, P. E. Thornton, F. M. Hoffman, S. Levis, P. J. Lawrence, J. J. Feddema, K. W. Oleson, and D. M. Lawrence (2010), Fire dynamics during the 20th century simulated by the Community Land Model, *Biogeosci. Discuss.*, 7(1), 565.
- Krezek-Hanes, C. C., F. Ahern, A. Cantin, and M.D. Flannigan (2011), Trends in large fires in Canada, 1959–2007, Canadian Biodiversity: Ecosystem Status and Trends 2010, Technical Thematic Report No. 6. Canadian Councils of Resources Ministers. Ottawa, ON. v + 48 p.
- Lamarque, J. F., J. Kiehl, G. Brasseur, T. Butler, P. Cameron-Smith, W. D Collins, W. J. Collins, C. Granier, D. Hauglustaine, and P. Hess (2005), Assessing future nitrogen deposition and carbon cycle feedback using a multimodel approach: Analysis of nitrogen deposition, *J. Geophys. Res.*, 110, D19303, doi:10.1029/2005JD005825.
- Langmann, B., B. Duncan, C. Textor, J. Trentmann, and G. R. van der Werf (2009), Vegetation fire emissions and their impact on air pollution and climate, *Atmos. Environ.*, 43(1), 107–116.
- Leff, B., N. Ramankutty, and J. A. Foley (2004), Geographic distribution of major crops across the world, *Global Biogeochem. Cycles*, 18, GB1009, doi:10.1029/2003GB002108.
- Lenihan, J. M., C. Daly, D. Bachelet, and R. P. Neilson (1998), Simulating broad-scale fire severity in a dynamic global vegetation model, *Northwest Sci.*, 72(4), 91–101.
- Lenihan, J. M., D. Bachelet, R. P. Neilson, and R. Drapek (2008), Simulated response of conterminous United States ecosystems to climate change at different levels of fire suppression, CO₂ emission rate, and growth response to CO₂, *Global Planet. Change*, 64(1-2), 16–25.
- Levine, J. S., W. R. Cofer III, D. R. Cahoon Jr, and E. L. Winstead (1995), A driver for global change, *Environ. Sci. Technol.*, 29(3), 120A–125A.
- Li, F., X. Zeng, and S. Lewis (2012), A process-based fire parameterization of intermediate complexity in a Dynamic Global Vegetation Model, *Biogeosciences*, 9(7), 2761–2780.
- Li, F., S. Lewis, and D. Ward (2013), Quantifying the role of fire in the Earth system—Part 1: Improved global fire modeling in the Community Earth System Model (CESM1), *Biogeosciences*, 10(4), 2293–2314.
- Liu, M., H. Tian, Q. Yang, J. Yang, X. Song, S. E. Lohrenz, and W.-J. Cai (2013), Long-term trends in evapotranspiration and runoff over the drainage basins of the Gulf of Mexico during 1901–2008, *Water Resour. Res.*, 49(4), 1988–2012, doi:10.1002/wrcr.20180.
- Liu, Y., J. Stanturf, and S. Goodrick (2010), Trends in global wildfire potential in a changing climate, *For. Ecol. Manage.*, 259(4), 685–697.
- Liu, Y., S. Goodrick, and J. Stanturf (2012), Future U.S. wildfire potential trends projected using a dynamically downscaled climate change scenario, *For. Ecol. Manage.*, 294(15), 120–135.
- Liu, Y., S. Goodrick, and W. Heilman (2013), Wildland fire emissions, carbon, and climate: Wildfire-climate interactions, *For. Ecol. Manage.*, doi:10.1016/j.foreco.2013.02.020.
- Lü, A., H. Tian, M. Liu, J. Liu, and J. M. Melillo (2006), Spatial and temporal patterns of carbon emissions from forest fires in China from 1950 to 2000, *J. Geophys. Res.*, 111, D05313, doi:10.1029/2005JD006198.
- Lu, C., and H. Tian (2013), Net greenhouse gas balance in response to nitrogen enrichment: Perspectives from a coupled biogeochemical model, *Global Change Biol.*, 19(2), 571–588.
- Marlon, J. R., P. J. Bartlein, C. Carcaillet, D. G. Gavin, S. P. Harrison, P. E. Higuera, F. Joos, M. J. Power, and I. C. Prentice (2008), Climate and human influences on global biomass burning over the past two millennia, *Nat. Geosci.*, 1(10), 697–702.
- Morton, D. C., G. J. Collatz, D. Wang, J. T. Randerson, L. Giglio, and Y. Chen (2013), Satellite-based assessment of climate controls on US burned area, *Biogeosciences*, 10(1), 247–260.
- Mouillet, F., and C. B. Field (2005), Fire history and the global carbon budget: A 1×1 fire history reconstruction for the 20th century, *Global Change Biol.*, 11(3), 398–420.
- Nelson, J. A., J. A. Morgan, D. R. LeCain, A. R. Mosier, D. G. Milchunas, and B. A. Parton (2004), Elevated CO₂ increases soil moisture and enhances plant water relations in a long-term field study in semi-arid shortgrass steppe of Colorado, *Plant Soil*, 259(1-2), 169–179.
- Nepstad, D. C., A. Verssimo, A. Alencar, C. Nobre, E. Lima, P. Lefebvre, P. Schlesinger, C. Potter, P. Moutinho, and E. Mendoza (1999), Large-scale impoverishment of Amazonian forests by logging and fire, *Nature*, 398(6727), 505–508

- Niklasson, M., and A. Granström (2000), Numbers and sizes of fires: Long-term spatially explicit fire history in a Swedish boreal landscape, *Ecology*, 81(6), 1484–1499.
- Norby, R. J., J. M. Warren, C. M. Iversen, B. E. Medlyn, and R. E. McMurtrie (2010), CO₂ enhancement of forest productivity constrained by limited nitrogen availability, *Proc. Natl. Acad. Sci. U.S.A.*, 107(45), 19,368–19,373.
- Payette, S., C. Morneau, L. Sirois, and M. Desponts (1989), Recent fire history of the northern Quebec biomes, *Ecology*, 70(3), 656–673.
- Pechony, O., and D. Shindell (2009), Fire parameterization on a global scale, *J. Geophys. Res.*, 114, D16115, doi:10.1029/2009JD011927.
- Pechony, O., and D. Shindell (2010), Driving forces of global wildfires over the past millennium and the forthcoming century, *Proc. Natl. Acad. Sci. U.S.A.*, 107(45), 19,167–19,170.
- Pfeiffer, M., and J. Kaplan (2012), SPITFIRE-2: An improved fire module for Dynamic Global Vegetation Models, *Geosci. Model Dev. Discuss.*, 5, 2347–2443.
- Prentice, I. C. (2010), The burning issue, *Science*, 330(6011), 1636–1637.
- Prentice, S., and D. Mackerras (1977), The ratio of cloud to cloud-ground lightning flashes in thunderstorms, *J. Appl. Meteorol.*, 16(5), 545–550.
- Randerson, J., H. Liu, M. Flanner, S. Chambers, Y. Jin, P. Hess, G. Pfister, M. Mack, K. Treseder, and L. Welp (2006), The impact of boreal forest fire on climate warming, *Science*, 314(5802), 1130–1132.
- Randerson, J., Y. Chen, G. R. van der Werf, B. M. Rogers, and D. C. Morton (2012), Global burned area and biomass burning emissions from small fires, *J. Geophys. Res.*, 117, G04012, doi:10.1029/2012JG002128.
- Ren, W., H. Tian, B. Tao, Y. Huang, and S. Pan (2012), China's crop productivity and soil carbon storage as influenced by multifactor global change, *Global Change Biol.*, 18(9), 2945–2957.
- Roy, D. P., L. Boschetti, C. O. Justice, and J. Ju (2008), The collection 5 MODIS burned area product—Global evaluation by comparison with the MODIS active fire product, *Remote Sens. Environ.*, 112(9), 3690–3707.
- Savage, M., and T. W. Swetnam (1990), Early 19th-century fire decline following sheep pasturing in a Navajo ponderosa pine forest, *Ecology*, 71(6), 2374–2378.
- Schultz, M. G., A. Heil, J. J. Hoelzemann, A. Spessa, K. Thonicke, J. G. Goldammer, A. C. Held, J. M. C. Pereira, and M. van het Bolscher (2008), Global wildland fire emissions from 1960 to 2000, *Global Biogeochem. Cycles*, 22, GB2002, doi:10.1029/2007GB003031.
- Simon, M., S. Plummer, F. Fierens, J. J. Hoelzemann, and O. Arino (2004), Burnt area detection at global scale using ATSR-2: The GLOBSCAR products and their qualification, *J. Geophys. Res.*, 109, D14S02, doi:10.1029/2003JD003622.
- Stocks, B. J., et al. (2002), Large forest fires in Canada, 1959–1997, *J. Geophys. Res.*, 107(D1), 8149, doi:10.1029/2001JD000484.
- Tansey, K., et al. (2004), A global inventory of burned areas at 1 km resolution for the year 2000 derived from spot vegetation data, *Clim. Change*, 67(2–3), 345–377.
- Tansey, K., J.-M. Grégoire, P. Defourny, R. Leigh, J.-F. Pekel, E. van Bogaert, and E. Bartholomé (2008), A new, global, multi-annual (2000–2007) burnt area product at 1 km resolution, *Geophys. Res. Lett.*, 35, L01401, doi:10.1029/2007GL031567.
- Tao, B., H. Tian, G. Chen, W. Ren, C. Lu, K. D. Alley, X. Xu, M. Liu, S. Pan, and H. Virji (2013), Terrestrial carbon balance in tropical Asia: Contribution from cropland expansion and land management, *Global Planet. Change*, 100, 85–98.
- Thomas, R. Q., C. D. Canham, K. C. Weathers, and C. L. Goodale (2009), Increased tree carbon storage in response to nitrogen deposition in the US, *Nat. Geosci.*, 3(1), 13–17.
- Thonicke, K., S. Venevsky, S. Sitch, and W. Cramer (2001), The role of fire disturbance for global vegetation dynamics: Coupling fire into a Dynamic Global Vegetation Model, *Global Ecol. Biogeogr.*, 10(6), 661–677.
- Thonicke, K., A. Spessa, I. Prentice, S. Harrison, L. Dong, and C. Carmona-Moreno (2010), The influence of vegetation, fire spread and fire behaviour on biomass burning and trace gas emissions: Results from a process-based model, *Biogeosciences*, 7(6), 1991–2011.
- Tian, H., X. Xu, M. Liu, W. Ren, C. Zhang, G. Chen, and C. Lu (2010), Spatial and temporal patterns of CH₄ and N₂O fluxes in terrestrial ecosystems of North America during 1979–2008: Application of a global biogeochemistry model, *Biogeosciences*, 7(9), 2673–2694.
- Tian, H., C. Lu, G. Chen, X. Xu, M. Liu, W. Ren, B. Tao, G. Sun, S. Pan, and J. Liu (2011), Climate and land use controls over terrestrial water use efficiency in monsoon Asia, *Ecohydrology*, 4(2), 322–340.
- Tian, H., G. Chen, C. Zhang, M. Liu, G. Sun, A. Chappelka, W. Ren, X. Xu, C. Lu, and S. Pan (2012), Century-scale responses of ecosystem carbon storage and flux to multiple environmental changes in the southern United States, *Ecosystems*, 15(4), 674–694.
- Venevsky, S., K. Thonicke, S. Sitch, and W. Cramer (2002), Simulating fire regimes in human-dominated ecosystems: Iberian Peninsula case study, *Global Change Biol.*, 8(10), 984–998.
- van Vuuren, D. P., P. L. Lucas, and H. Hilderink (2007), Downscaling drivers of global environmental change: Enabling use of global SRES scenarios at the national and grid levels, *Global Environ. Change*, 17(1), 114–130.
- van der Werf, G. R., J. T. Randerson, L. Giglio, G. J. Collatz, P. S. Kasibhatla, and A. F. Arellano Jr (2006), Interannual variability in global biomass burning emissions from 1997 to 2004, *Atmos. Chem. Phys.*, 6(11), 3423–3441.
- van der Werf, G. R., W. Peters, T. T. van Leeuwen, and L. Giglio (2013), What could have caused pre-industrial biomass burning emissions to exceed current rates?, *Clim. Past*, 9(1), 289–306.
- Wagner, C. V. (1988), The historical pattern of annual burned area in Canada, *The Forestry Chronicle*, 64(3), 182–185.
- Wallenius, T. H., T. Kuuluvainen, and I. Vanha-Majamaa (2004), Fire history in relation to site type and vegetation in Vienansalo wilderness in eastern Fennoscandia, Russia, *Can. J. For. Res.*, 34(7), 1400–1409.
- Wang, Z., J. Chappelaz, K. Park, and J. Mak (2010), Large variations in Southern Hemisphere biomass burning during the last 650 years, *Science*, 330(6011), 1663–1666.
- Westerling, A. L., and T. W. Swetnam (2003), Interannual to decadal drought and wildfire in the western United States, *Eos Trans. AGU*, 84(49), 545.
- Westerling, A. L., H. G. Hidalgo, D. R. Cayan, and T. W. Swetnam (2006), Warming and earlier spring increase western US forest wildfire activity, *Science*, 313(5789), 940–943.
- Xu, X., H. Tian, C. Zhang, M. Liu, W. Ren, G. Chen, C. Lu, and L. Bruhwiler (2010), Attribution of spatial and temporal variations in terrestrial methane flux over North America, *Biogeosci. Discuss.*, 7(4), 5383–5428.
- Zhang, C., H. Tian, Y. Wang, T. Zeng, and Y. Liu (2010), Predicting response of fuel load to future changes in climate and atmospheric composition in the Southern United States, *For. Ecol. Manage.*, 260(4), 556–564.